Published in final edited form as:
J Neural Eng. 2013 December ; 10(6): 066013. doi:10.1088/1741-2560/10/6/066013.

Facilitation of Memory Encoding in Primate Hippocampus by a Neuroprosthesis that Promotes Task Specific Neural Firing

Robert E. Hampson[1], **Dong Song**[2], **Ioan Opris**[1], **Lucas M. Santos**[1], **Dae C. Shin**[2], **Greg A. Gerhardt**[3], **Vasilis Z. Marmarelis**[2], **Theodore W. Berger**[2], and **Sam A. Deadwyler**[1]

[1]Department of Physiology and Pharmacology, Wake Forest University School of Medicine, Winston-Salem, NC

[2]Department of Biomedical Engineering, University of Southern California, LA, CA

[3]Department of Anatomy and Neurobiology, University of Kentucky, Lexington, KY

Abstract

Objective—Memory accuracy is a major problem in human disease and is the primary factor that defines Alzheimer's', aging and dementia resulting from impaired hippocampal function in medial temporal lobe. Development of a hippocampal memory neuroprosthesis that facilitates normal memory encoding in nonhuman primates (NHPs) could provide the basis for improving memory in human disease states.

Approach—NHPs trained to perform a short-term delayed match to sample (DMS) memory task were examined with multi-neuron recordings from synaptically connected hippocampal cell fields, CA1 and CA3. Recordings were analyzed utilizing a previously developed nonlinear multi-input multi-output (MIMO) neuroprosthetic model, capable of extracting CA3-to-CA1 spatiotemporal firing patterns during DMS performance.

Main Results—The MIMO model verified that specific CA3-to-CA1 firing patterns were critical for successful encoding of Sample phase information on more difficult DMS trials. This was validated by delivery of successful MIMO-derived encoding patterns via electrical stimulation to the same CA1 recording locations during the Sample phase which facilitated task performance in the subsequent delayed Match phase on difficult trials that required more precise encoding of Sample information.

Significance—These findings provide the first successful application of a neuroprosthesis designed to enhance and/or repair memory encoding in primate brain.

Keywords

Hippocampal neuron; spike train; memory encoding; nonlinear model; patterned electrical stimulation; prosthesis; prosthetic; memory facilitation; memory retention; nonhuman primate

INTRODUCTION

Memory deficits in humans are constantly related to an inability to recall items previously exposed in different contexts or to utilize the same items for different purposes (Jenkins and Ranganath 2010; Tubridy and Davachi 2011). It has been known from the initial

*Corresponding Author: Dr. Sam A. Deadwyler, Wake Forest University School of Medicine, Department of Physiology and Pharmacology, Medical Center Boulevard, Winston Salem NC 27157, ph: 336-716-8540, fax: 336-716-8628, sdeadwyl@wfubmc.edu.

The authors declare no competing financial interests

characterization of factors which affect proper recall of information that after an intervening period of lack of exposure to the item, correct retention or retrieval of the item is dependent on the strength of encoding of the information at the time of the initial exposure (Downes et al. 2002; Moscovitch et al. 2006). Understanding the neural basis of memory processes has progressed to the level of knowing that certain brain systems must be operative in order for effective encoding and subsequent retention to occur, and that many types of memory are different and utilize different structures related to functional behavioral endpoints (Naya and Suzuki 2011).

In the mammalian brain the hippocampus has been shown to be the most important structure involved in the encoding and retention of new information in cognitive processes (Eichenbaum and Fortin 2003; Tulving 2002). It is well documented that impairment of the functional status of the hippocampus in human disease states leads to memory deficits that are detrimental to normal function, and in addition such impairment has become the hallmark of brain aging and deterioration as exhibited by Alzheimer's patients (Carmichael et al. 2012; Gemmell et al. 2012). Unlike other approaches with neural prosthetics to rectify altered brain function, the recovery or replacement of memory is an objective that cannot be accomplished until we understand how the hippocampus performs the encoding of information to be retained at a later time (Manns et al. 2007; Pastalkova et al. 2008). Initial results from this laboratory have shown that a critical feature necessary for retention of item-specific cognitive information is the pattern of firing across distinct cell groupings within hippocampus (layers CA3 and CA1) that are synaptically connected and communicate during the encoding process. The ability to monitor activity in these areas in rodents while processing information in a memory task using an online nonlinear multi-input multi-output (MIMO) model (Berger et al. 2011), provided the means to extract "strong" and "weak" codes or patterns of firing associated with correct or error trials in the same testing sessions (Hampson et al. 2012d). The relevance of the MIMO derived firing patterns was demonstrated by injection of those same model predicted patterns in the form of electrical stimulation into the hippocampal output layer, CA1, which facilitated retention of task-specific information in the same manner as when the patterns were generated spontaneously in CA1 via synaptic input from CA3 (Hampson et al. 2012c).

The current study extends this same approach to assessing hippocampal involvement in the encoding of relevant information by nonhuman primates (NHPs) engaged in a more complex cognitive memory task requiring retention of several stimulus features as well as trial specific information to perform correctly as demonstrated in several prior reports (Deadwyler et al. 2007; Hampson et al. 2004; Hampson et al. 2009; Porrino et al. 2005). In order to implement the previously successful multi-input-multi-output (MIMO) model prosthesis (Hampson et al. 2012a) for recovery of memory loss in primate brain, it is necessary to demonstrate how this model enhances normal memory under conditions where retrieval of information is less effective in more difficult task-related contexts (Berger et al. 2011; Berger et al. 2012; Hampson et al. 2012c; Hampson et al. 2012d). Successful application in prior studies served as the basis for testing the MIMO model in primate hippocampus utilizing interposed delivery of extracted patterns of successful CA3-CA1 cell firing as electrical stimulation to the same regions.

The current results here show that application of the same MIMO model derived stimulation, when applied to hippocampal CA3&CA1 subregions in NHPs provides a high degree of facilitation of performance across different types of memory challenges and therefore satisfies the same criteria to serve as a neural prosthesis in primate brain, as previously demonstrated in prefrontal cortex of NHPs (Hampson et al. 2012a). These results provide the first instance of application of a neuroprosthesis designed specifically for enhancing memory in primate brain, and as such indicate the potential efficacy for

recovering hippocampal dysfunction related to memory loss disease states and aging in humans (Riddle and Lichtenwalner 2007).

METHODS

All animal procedures were reviewed and approved by the Institutional Animal Care and Use Committee of Wake Forest University, in accordance with U.S. Department of Agriculture, International Association for the Assessment and Accreditation of Laboratory Animal Care, and National Institutes of Health guidelines.

Cognitive Memory Task

Four nonhuman primate (NHP) subjects (rhesus, *Macaca mulatta*) were trained for at least 2 years to perform the visuospatial delayed-match-to-sample (DMS) task (Hampson et al. 2012a; Opris et al. 2012a; Opris et al. 2012b) for juice rewards (Fig. 1a) and all met a criterion performance level stable for at least 1 year. Animals were seated in a primate chair with a shelf-counter in front of them facing a large display screen during task performance. Right hand position on the counter top was tracked via a UV-fluorescent reflector affixed to wrist and illuminated with a 15 W UV lamp. Hand position and movement was detected by a small LCD camera positioned 30 cm above the hand, digitized using a Plexon Cineplex scanner connected to a behavioral control computer, and displayed as a bright yellow cursor on the projection screen. Trials were initiated by the animal placing the cursor inside a centrally-placed yellow circle or red square, either which constituted the “Start signal” for a given trial. Following trial initiation by response to the Start Signal, a single image was presented randomly on the screen as the Sample stimulus constituting the Sample Presentation (SP) phase of the task. The different visual features of the Start signal presented on a trial conveyed the type of response contingency with respect to the Sample stimulus (SP) after response to the Start signal. If the Start signal was 1) a yellow circle, it indicated Object type trials in which the Sample stimulus clip art image itself was to be responded to in the Match Phase irrespective of screen position; or 2) a red square, it indicated Spatial type trials in which the correct response was the screen position in which the Sample Stimulus was presented irrespective of which clip-art image occupied that same position in the Match Phase. Completion of the Sample phase of the task required placement of the cursor into the displayed clip-art image, and was designated the *Sample Response* (SR). The SR initiated the *Delay* interval phase of the trial, in which the screen was blanked for 1–90s, randomly determined on a trial-to-trial basis. Timeout of the Delay interval was signaled by the automatic onset of the Match phase of the task, consisting of the simultaneous display of 2–7 trial unique images, including the Sample image, all at separate randomly selected spatial locations on the screen with at least one screen position always left blank. Placement of the cursor into one of the images constituted a “Match Response” (MR) – however, as stated above, selection of the correct image was dictated by the trial type signaled by the Start Signal as noted above for cursor placement in the Match phase: 1) into the same image as the Sample stimulus on Object trials, or 2) into the same screen location where the Sample stimulus appeared irrespective of image characteristics on Spatial trials. Correct responses produced a juice reward delivered via a sipper tube located near the animal’s mouth and blanked the screen. Placement of the cursor into one of the non-match (distracter) images or a different screen location constituted a nonmatch-error response and caused the screen to blank without reward delivery. Trials during the session were separated by a minimum of 10 sec in which the Start signal was presented following termination of the Match phase of the prior trial. All clip-art images presented (sample and distracters) were unique for each trial in the session (100–150 trials) and were selected randomly from an image reservoir (n=5000) updated every month (Hampson et al. 2004). All subjects were trained to overall performance levels of 70–75% correct on the least difficult trials with

graded performance on trials with increased delays and number of images in the above described version of the DMS task.

Surgery

Animals were surgically prepared with cylinders for daily attachment of a microelectrode manipulator over the specified brain regions of interest. During surgery animals were anesthetized with ketamine (10 mg/kg), then intubated and maintained with isoflurane (1–2 % in oxygen 6 ℓ/min). Recording cylinders (Crist Instruments, Hagerstown, MD) were placed over 20 mm diameter craniotomies for electrode access (Hampson et al. 2012a; Opris et al. 2011; Opris et al. 2012a; Opris et al. 2012b) to stereotaxic coordinates of the Hippocampus (12 mm anterior relative to interaural line and 12 mm lateral to midline/vertex) previously shown by PET imaging (Porrino et al. 2005) to become activated during task performance (Fig. 1b). Two titanium posts were secured to the skull for head restraint with titanium screws embedded in bone cement. Following surgery, animals were given 0.025 mg/kg buprenorphine for analgesia and penicillin to prevent infection. Recording cylinders were disinfected thrice weekly with Betadine during recovery and daily following task recording.

Recording from Hippocampus

Electrophysiological procedures and analysis utilized the 64 channel MAP Spike Sorter by Plexon, Inc (Dallas, TX). Customized tetrode arrays (Santos et al 2012) were manufactured specifically for recording spatially distinct locations in the CA3 and CA1 cell fields in primate hippocampus (Hampson et al 2004) such that multi-cell (n>12) recordings could be obtained from each anatomically distinct location. The Schaefer collateral projections from CA3 to CA1 are ubiquitous enough to insure that the locations recorded from in CA3 were likely connected synaptically to the locations recorded from in CA1 in each Tetrode pair located in the same mediolateral plane or “chip” of hippocampus in two distinct anterior-posterior locations as shown in Figures 1 & 6. This tetrode arrangement insured that only cells in CA3 and CA1 were isolated and recorded, since the appearance of activity on each vertically inserted probe occurred at depths of insertion for CA1 that required prior traversal through cell layer CA3 placed in the same cross-sectional plane of hippocampus as shown in Figure 1B.

Identification of CA1 and CA3 Hippocampal Cell Layers

Electrode locations in the appropriate cell layers with individual tetrodes was validated by placement using the same coordinates in different animals to ascertain localization in both CA1 and CA3 cell layers. These placements were verified on a daily basis and were utilized as markers for correct placement. Histological verification was confirmed in 3 animals euthanized after this study was completed. Statistical analyses also determined whether there were differences in firing rates for cells in different layers (i.e. CA1 vs. CA3) during activation in the Sample and Match Phases of the task.

Data Analysis

Task performance was determined for each animal (n=4) as % correct responses within trial groups sorted according to duration of delay and number of images presented in Match phase (Figure 1C&D). Number of correct and incorrect trials were summed, and percentage of correct responses computed within sessions, with average performance computed across a minimum of three sessions (Hampson et al. 2012a). Recordings of multiple CA3 and CA1 neuron firings on individual trials (Hampson et al. 2004) during the Sample and Match phases of the DMS task were summed within 100 ms bins, and accumulated across trials within a session for display as perievent histograms (PEHs) of mean firing rate (i.e. spikes/

sec) relative to the Sample or Match events (Figures 2&3). Cell types were identified as regular firing hippocampal cells in terms of baseline (nonevent) firing rate (Hampson et al. 2004; Opris et al. 2009; Opris et al. 2011) and peaks on single trials in PEHs derived for intervals of ± 2.0s relative to the onset of the screen image display (0.0s) in the Sample and Match phases of the task (Figures 2&3). Significant firing peaks were identified by maximum firing rate ± 0.5s relative to the DMS event by standard score (Z = [peak − baseline firing rate] ÷ std. dev. of baseline, $z>3.09$ values indicated significant ($p<0.001$) peak increase in firing rate). Firing rates for simultaneously recorded CA1 and CA3 neurons were analyzed in 100 ms bins over ± 2.0 s relative to the time of initiation (0.0s) of the Sample and Match phases of the task. Neurons were only included in the analysis if their firing rates were significantly elevated (Z-scores, ANOVA F test $p < 0.01$) relative to the pre-event screen presentation baseline period (−2.0 to 0.0s). The correspondence of firing between cells in different layers was tested via comparison of trial-based histograms (TBHs) spanning more than one task event within a phase to construct templates related to how the hippocampus encoded trial specific information. PEHs demarcated firing differences for individual events and to provide the basis for nonlinear model analyses of firing during particular Sample and Match types of events within a given trial.

MIMO Model for Hippocampal Neural Activity during the DMS Task

Prior studies (Berger et al. 2011; Hampson et al. 2012a) have shown that a multi-input/multi-output (MIMO) nonlinear dynamic model applied to spatiotemporal patterns of multiple recordings from rodent hippocampal CA1 and CA3 neurons capable of extracting patterns of firing related to successful performance of a nonmatch to sample memory task, could be used to facilitate and recover performance when administered to the same locations as patterns of electrical pulses (Berger et al. 2011; Hampson et al. 2012a; Hampson et al. 2012c; Hampson et al. 2012d). The same structure MIMO model as in the earlier studies has been adapted (with coefficients unique to the current data) was applied to the current data set to assess the spatiotemporal nonlinear dynamics underlying spike train-to-spike train transformations between CA3 and CA1 cells to predict CA1 output firing patterns from input patterns of CA3 neural activity via the well characterized Shaffer collateral synaptic connectivity between these areas in primate hippocampus (Deguchi et al. 2011; Klausberger and Somogyi 2008). This type of general Volterra kernel-based nonlinear model has been applied in other formats which have also been shown to be effective in rodents (Marmarelis et al. 2012; Marmarelis et al. 2013). The MIMO version of the model was applied here to the data recorded by the multiple tetrode probes in NHPs performing the DMS task described in Figure 1, and is structurally similar to the model shown to facilitate DMS performance when applied to NHP prefrontal cortical neurons in a prior study (Hampson et al. 2012a).

RESULTS

Adult, male rhesus macaques (n=4) were trained to perform the combined delayed-match-to-sample (DMS) task shown in Figure 1 (Hampson et al. 2011; Opris et al. 2012b), by making hand tracking cursor movements on the screen in front of them to obtain a juice reward for selection of either the same Sample, image or location, in the Match phase which varied randomly from 1 of 8 different positions on the screen on each trial. The Start Signal for a given trial indicated whether the animal was required to remember either (1) which Sample clipart image (Object trial) was presented or, (2) which one of the 8 positions on the screen the Sample image was presented (Spatial trial). Animals rewarded for the appropriate selection in the subsequent Match phase of the same trial. Key variables in the task that changed randomly on a trial-by-trial basis were, the number of images (2–7) presented in the Match phase, the duration of the Sample-to-Match phase delay interval (1 to 90 sec) and

placement of the Sample image randomly on the screen in one of 8 positions in the Match phase (after the delay interval), all of which have been characterized in previous studies (cf. Hampson et al. 2012a). Several important cognitive features such as attention, short-term memory, cognitive workload, reward expectancy, as well as a "decision process" in the Match phase, associated with performance of the task have previously been shown to be related to task related neuron activation in different brain regions (Hampson et al. 2010; Hampson et al. 2012b; Opris et al. 2011). In addition the specificity of single neuron firing in the hippocampus in the same task including encoding of image features presented in the Sample phase has been documented in prior studies (Hampson et al. 2004). However, prior work in NHPs did not employ simultaneous multi-cell recording in hippocampus with spatiotemporal specificity in relation to CA3-CA1 activation or synchronous firing under trial specific conditions as described next.

Hippocampal Neural Activity during Stimulus Encoding in the Sample Phase

Hippocampal neuron firing during the Sample phase of the DMS task reflects the degree of stimulus encoding required for accurate recall and selection of the proper target in the Match phase of the DMS task after an interposed variable delay period (see Figure 1A). Figure 2A shows that neurons in CA1 and CA3 exhibited significantly increased peaks in average firing rate computed across all animals during the 3 critical events in the Sample phase: Trial Start signal-*Strt* ($z = 5.21–27.58$, $p<0.001$), Sample (Image) Presentation-*SP* ($z = 4.13–22.40$, $p<0.001$), and the behavioral Response to the Sample image-*SR* ($z = 3.42–12.68$, $p<0.001$). An important feature regarding the significance of this phase of the task in addition to the three distinct events for encoding Sample information was the significantly elevated overall firing above baseline levels (dotted lines in Figure 2A) for neurons in both CA1 and CA3 ($z = 4.81$, $p<0.001$) in a manner that was different with respect to a) the type of trial and 2) the subsequent consequence on correct or error trials. Figure 2B shows this differentiation for all 4 possible outcomes with respect to trial type and performance. What is very important is the fact that mean firing rates in CA1 and CA3 were significantly different with respect to the Strt and SP events on Object vs. Spatial trials (TS: $F(1,7239) = 11.14$, $p<0.001$, SP: $F(1,7239) = 8.22$, $p<0.01$), however mean firing rates during the SR were similar in both CA1 and CA3 with respect to subsequent correct vs. error performance in the Match phase (Figure 2B) of the same trial (SR: $F(1,7239) = 5.20$, N.S.)

Hippocampal Neural Activity during Target Selection in the Match Phase

The basis for effective CA1 and CA3 encoding activity in the Sample phase of the task culminated in the selection of either the same Sample image (Object trial) or the same Sample screen location (Spatial trial) in the Match phase of the DMS task. Figures 3A&B show the average firing rates of the same CA3 and CA1 neurons described in Figure 2 in the subsequent two primary events in the Match phase of the same trials. This includes: 1) onset of the match screen image presentation (MP) and 2) movement of the cursor into a screen location selection as the match response (MR). The MR determined a correct or error trial with respect to the previously presented Sample information (Figure 2B). Figure 3A shows mean firing rate of CA1 and CA3 neurons at the onset of the match phase (MP, $z = 5.59–22.17$, $p<0.001$) continuous through initiation and completion of the MR ($z = 4.11–40.79$, $p<0.001$). The average firing rate of CA1 and CA3 neurons associated with performance differences for both types of trial (Object and Spatial) is shown for both the MP and MR events in Figure 3A. A display of Match phase average peak firing rates during the same events is shown in Figure 3B, Peak firing in CA1 and CA3 during the MR distinguished correct vs. error performance with respect to both Object and Spatial trials with CA1 neurons exhibiting higher rates than CA3 neurons (CA1: $F(1,7239) = 7.50$, $p<0.01$, CA3: $F(1,7239) = 11.16$, $p<0.001$) under those conditions. There were also much lower firing

rates during MP compared to MR in both CA1 and CA3 and less difference with respect to firing on correct vs. error trials (Figure 3B).

These features are rearranged in Figure 4 to show the correspondence between SR and MR firing on each type of trial and its success or failure with respect to being a correct or error outcome. Figure 4 shows that Match phase firing was portioned in the same manner as Sample phase firing on correct vs. error trials. This provides confirmation that significantly increased firing in the Sample phase at the time of the SR, was the basis for subsequent correct MR selection in the Match phase. It is clear that the ratios of mean firing on correct and error trials in CA1 and CA3 were similar for the critical events in each phase of the task (SR and MR). Object trials were encoded and responded to almost identically in each area while more differentiation between correct and error trials occurred in CA3 during the SR in the Sample phase for Spatial trials compared to MR firing where CA1 neurons showed more distinct differentiation of average firing rate (CA1: $F(1,7239) = 19.83$, $p<0.01$, CA3: $F(1,7239) = 16.16$, $p<0.001$).

Hippocampal Sample Phase Firing with Respect to Retention across Variable Delay Intervals and Number of Images in the Match Phase

Figure 5A&B shows the systematic comparison of correct vs. error performance as a function of mean firing rate during the SR on Object vs. Spatial trials with different durations of intervening delays and number of images in the Match phase. Firing of CA1 and CA3 neurons was significantly higher on correct vs. error trials for both Object and Spatial trials at delays of 1–30s and 2–5 images (Figure 5A&B), However, on Object trials with longer delays (31–40s) and more Match phase images (6–7), SR firing was significantly increased in both areas (CA1: $F(3,7239) = 12.68$, $p<0.001$, CA3: $F(3,7239) = 13.11$, $p<0.001$) relative to trials with shorter delays. Delays > 30s and 6–7 images were not employed on Spatial trials since those parameters decreased performance to near chance levels (Figure 1C&1D). The nearly linear relationship with respect to trial difficulty and Sample firing intensity shown in Figure 5 for all trial parameters provides direct evidence that hippocampal SR firing rate (Figure 2) determined whether the information was available on the same trial for use later in the Match phase. Clearly if the duration of the delay was short (< 11.0s), or number of Match phase images few (2–3) as on “easy” trials (Figure 1C&D), SR firing rates in CA1 and CA3 were lower than SR rates required for correct choices on more “difficult” trials with increased delays (20–40s) or number of images (4–7) (CA1: $F(2,7239) = 11.93$, $p<0.001$, CA3: $F(3,7239) = 12.47$, $p<0.001$). The fact that nearly the same relations to different trial parameters existed for both CA1 and CA3 firing is consistent with earlier demonstrations of these same relations (Hampson et al 2004) and supports the notion that both areas were encoding the same type of Sample information via the synaptic connections between the two cell layers (Deguchi et al. 2011; Klausberger et al. 2008). Figure 5 shows that accurate retention of trial specific information was dependent on increased CA1 and CA3 neuron firing during the SR which was well above firing levels on error trials with the same delays and number of Match phase distracter images.

MIMO Model Extraction of Successful Hippocampal Processing of Sample Information

The MIMO model was applied as shown in Figure 6 to the same type of hippocampal neuron firing recorded during the Sample phase of the DMS task. The MIMO model provided the identification of spatio-temporal patterns from neurons recorded in CA3 that were transferred to synchronize with neurons recorded in CA1 (Berger et al. 2011; Marmarelis 2004; Marmarelis and Berger 2005; Song et al. 2009). These were formulated as the estimation of the MIMO model decomposed into a series of multi-input, single-output

(MISO) models with physiologically identifiable structure expressed by the following equations:

$$w=u(k,x)+a(h,y)+\varepsilon(\sigma), y=\begin{cases} 0 & \text{when} w<\theta \\ 1 & \text{when} w \geq \theta \end{cases}$$

The variable *x* represents input (CA3) spike trains; *y* represents output (CA1) spike trains. The hidden variable *w* represents the pre-threshold membrane potential of the output neurons, and is equal to the summation of three components: 1) post-synaptic potential *u* caused by input spike trains, 2) the output spike-triggered after-potential *a*, and 3) a Gaussian white noise ε with standard deviation σ. The noise term models both intrinsic noise of the output neuron and the contribution of unobserved inputs. Threshold, θ, determines when an output spike is generated. Two nonlinear kernels complete the equation: as shown below.

Feedforward kernel *k* indicates transformation from *x* (input) to *u* (membrane potential), and can be expressed as a Volterra functional series of *x*, as follows:

$$\begin{aligned} u(t)=k_0+\sum_{n=1}^{N}\sum_{\tau=0}^{M_k}k_1^{(n)}(\tau)x_n(t-\tau)+\sum_{n=1}^{N}\sum_{\tau_1=0}^{M_k}\sum_{\tau_2=0}^{M_k}k_{2s}^{(n)}(\tau_1,\tau_2)x_n(t-\tau_1)x_n(t-\tau_2) \\ +\sum_{n_1=1}^{N}\sum_{n_2=1}^{n_1-1}\sum_{\tau_1=0}^{M_k}\sum_{\tau_2=0}^{M_k}k_{2x}^{(n_1,n_2)}(\tau_1,\tau_2)x_{n_1}(t-\tau_1)x_{n_2}(t-\tau_2) \\ +\sum_{n=1}^{N}\sum_{\tau_1=0}^{M_k}\sum_{\tau_2=0}^{M_k}\sum_{\tau_3=0}^{M_k}k_{3s}^{(n)}(\tau_1,\tau_2,\tau_3)x_n(t-\tau_1)x_n(t-\tau_2)x_n(t-\tau_3)+\ldots \end{aligned}$$

The zeroth order kernel, k_0, is the value of *u* with no input. First order kernels, $k_1(n)$, describe the linear relation between the n^{th} input x_n and *u*. Likewise, second and third order self-kernels, $k_{2s}^{(n)}$, and $k_{3s}^{(n)}$, describe the 2^{nd} and 3^{rd} order nonlinear relation between n^{th} input x_n and *u*, respectively. Second order cross-kernels $k_{2x}^{(n1,n2)}$ reflect the 2^{nd} order nonlinear interactions between each unique pair of inputs (x_{n1} and x_{n2}) as they affect *u*. N is the number of inputs. M_k denotes the memory length of the feedforward process. *t* is a given (current) time point within the spike train, while τ identifies the time points of the most recent (τ or τ_1), second most recent (τ_2), and third most recent (τ_3) preceding spikes.

The feedback kernel *h* describes the transformation from *y* (output) to *a* (afterhyperpolarization) and can be expressed as:

$$a(t)=\sum_{\tau=1}^{M_h}h(\tau)\,y(t-\tau)$$

where *h* is the linear feedback kernel and M_h is the memory length (time in ms) of the feedback process. In summary, the model describes the temporal relationship of up to three prior neural CA3 spikes, within and across spike trains, interact to determine the sequence of CA1 spike trains comprising outputs, taking into account differing noise level and output spike-triggered feedback (the latter due to circuitry and/or membrane biophysics), as well as neuron-specific differences in thresholds.

Analyses included extraction of first, second and third order temporal firing recorded by the dual tetrodes inserted into both layers on multiple recording sessions in order to extract

relevant spatiotemporal patterns of CA3 to CA1 activity related to successful image selection during the Match phase of the task. The model defined inputs as firing from neurons in CA3 and outputs as similar longitudinally located CA1 neurons which determined the nature of the output patterns extracted by the MIMO model. In this manner model output predictions of CA1 firing related to successful performance were monitored online from tetrodes in CA3 during the task as shown in Figure 6, to detect when successful trials were about to be completed by appropriate target selection (MR).

MIMO Model Extraction of Trial Specific CA1 Neuron Firing Patterns Related to CA3 Neuron Firing

Prior investigations applying MIMO model derived patterns of electrical stimulation pulses to the rodent hippocampus provided the means to enhance performance in normal circumstances and overcome deficits induced by pharmacologic disruption in rodents trained to perform a short-term memory task (Berger et al. 2011; Hampson et al. 2012c). The approach employed here in NHPs was identical in that simultaneous spatiotemporal multi-neuron recordings from CA3 and CA1 were employed to construct a MIMO model capable of predicting CA1 output firing from online-monitored CA3 inputs to the MIMO model as shown in Figure 6. These patterns were derived specifically from simultaneous CA3 neuron firing related to the TS, SP and SR task events. Figure 7A shows not only trial-by-trial firing of a single CA3 neuron on both Spatial and Object trials (see Figure 2), but averaged PEHs across CA3 neurons which demonstrated mean firing responses to TS, SP and SR events even with individual trial and neuron variability. Representative Object and Spatial trial mean firing patterns for CA3 ensembles are paired with similar displays for CA1 neuron ensembles over the same time base via a graphic, 'heat-map' representation of the individual spike train firing of 16 neurons on a single trial. The MIMO model was used to predict specific CA1 firing patterns that coincided with CA3 firing on both Object and Spatial trials during the Sample phase of the task (Figure 7B). The upper two traces in Figure 7C show similar representations of the real-time recorded CA3 ("Input") and CA1 ("Actual") multi-neuron spike train firing patterns from single Object and Spatial trials. The MIMO "Predicted" CA1 output pattern shown at the bottom was produced by the developed MIMO model from the CA3 (Input) spike trains shown above, and demonstrates the similarity to real time (Actual) recorded CA1 neuron firing over the same time period for both Object and Spatial trials.

The same MIMO model was applied to specific performance conditions for both types of trials (Object and Spatial) in which Sample phase CA3 and CA1 firing in the time frame from SP to SR (dashed red outline in Figure 7C) was associated with correct or incorrect (error) consequences on trials with the same parameters. This is shown in Figure 8 in which MIMO model derived 'strong code' (correct) and 'weak code' (error) firing patterns predicted performance for CA1 on Object and Spatial type trials as a function of delay (upper) and number of images in the Match phase (lower). Figure 8 validates the notion that normal performance over all conditions was a combination of strong and weak code occurrences since performance on strong code trials was above (by Delay: $F(1,3106) = 12.90$, $p<0.001$, by Images: $F(1,3106) = 13.48$, $p<0.001$), and on weak code trials was below (by Delay: $F(1,3106) = 11.73$, $p<0.001$, by Images: $F(1,3106) = 10.74$, $p<0.001$) the average performance curve in which trials were not segregated as a function of Sample phase MIMO code strength. The similarity and generality of this type of encoding was demonstrated in a consistent manner across different NHPs as shown in the Supplemental Figure A (available online) in which strong and weak codes are shown for all 4 animals on Object trials and Spatial trials.

Effects of MIMO Derived Stimulation on Performance of the DMS Memory Task

The extraction of MIMO derived strong and weak code CA1 firing patterns was translated to a means of injecting these patterns extraneously via multi-channel electrical stimulation of the same CA1 regions delivered on trials in which the MIMO model did not detect the precursor CA3 firing for Strong codes. This approach has been used previously in rodents (Berger et al. 2011; Hampson et al. 2012c; Hampson et al. 2012d) and was also used successfully in prior studies with NHPs performing this same DMS task in which MIMO formulated Strong code stimulation patterns were delivered to prefrontal cortex in the Match phase (Hampson et al. 2012d). If CA3 firing derived by the MIMO model on a given trial was not a Strong code, then previously derived CA1 Strong code firing patterns from the same animal (e.g. Figure 8) were delivered within 50 msec in the form of electrical pulses to the same CA1 recording sites. Electrical pulses consisted of biphasic constant-current square waves, 0.5 ms per phase triggered by the same MIMO coefficients derived for Strong codes (Berger et al. 2011; Hampson et al. 2012c) at intensities (10–50 μA) that produced moderate and reliable local field potentials at the same recording locations. MIMO derived Strong code stimulation patterns were delivered only during the Sample phase of the task following the SP and immediately prior to and during the SR as shown in Figures 6&8, to restrict Strong code stimulation to the information required to be encoded for retention on the immediate trial type. MIMO stimulation was delivered randomly on 30–50% of trials in each session which allowed comparison with non-stimulated trials in terms of correct or incorrect performance under the same conditions.

Figure 9 demonstrates the effectiveness of the MIMO derived CA1 stimulation patterns delivered to all 4 NHPs in which facilitation of performance was directly related to trials with increased difficulty with respect to both delay and number of images, in the same manner that normal hippocampal cell firing and performance varied across the same parameters (Figure 5). Delivery of the MIMO Strong code stimulation pattern facilitated performance on trials in all 4 NHPs and the degree of performance improvement was more pronounced on trials with increased delay duration (Delay): $F(3,1682) = 7.04$, $p<0.001$) and/or increased number of Match distracter images (# images: $F(5,1682) = 5.13$, $p<0.001$). These changes produced by delivery of strong codes during the Sample phase resembled the same profile performance changes that occurred normally on trials where the MIMO model extracted natural strong code firing patterns as shown in Figure 8 (by Delay: $F(3,3106) = 7.67$, $p<0.001$, by Images: $F(5,3106) = 9.04$, $p<0.001$). In addition, even though performance on stimulation trials remained proportionately decreased as a function of increase in trial difficulty, the decrease was not the same magnitude as on non-stimulated trials with the same parameters (Figure 9).

Complementary to these findings was the demonstration of the specificity of MIMO SR stimulation which differentially enhanced mean performance across all animals as a function of the type of trial (Object or Spatial) presented, as shown in Figure 10. It is clear that overall normal performance was more difficult on Spatial vs. Object trials and that delivery of trial specific MIMO strong code stimulation significantly enhanced performance on longer delay Spatial trials ($F(3,1682) = 4.18$, $p<0.01$). Figure 10 also shows an important control for the specificity of MIMO strong code stimulation in which the derived model coefficients of the MIMO kernels ('*k*', in the model equation) were 'scrambled' i.e. applied randomly, to individual CA1 neuron firing patterns. These patterns were delivered with exactly the same stimulation parameters (pulse duration and intensity) at the same time during the Sample phase of the task and on the same types of trials. The scrambled Strong code stimulation patterns did not enhance performance and had essentially no effect ($F(1,1682) = 2.42$, N.S.) on normal behavior on the same types of trials in which the delivery of the actual MIMO strong code patterns was highly effective (Figure 10). The fact

that scrambling the Strong code MIMO coefficients eliminated performance facilitation with respect to both a) the type of trial (Object and Spatial) as well as b) particular parameters (delay and # of images), verifies that the strong code *pattern* of MIMO-derived stimulation, not just electric current, applied during Sample phase was the critical event that facilitated performance of the DMS task. In addition the fact that the scrambled strong code patterns did not significantly disrupt normal performance (Figure 10) indicates that altering the coefficients in this manner only eliminated a more proficient pattern of CA3-CA1 cell activation, and did not disrupt cell firing enough to produce errors or 'weak codes' (Figure 8).

Application of MIMO-Stimulation as a Memory Prosthetic to Enhance Hippocampal Encoding

From the perspective of recovery of function involving memory deficits in primate brain, these results in which MIMO model derived stimulation enhanced Sample phase encoding in NHPs (Figures 9&10), provides a basis for application of this same MIMO model to human disease and brain aging conditions in which memory is reduced as a result of impaired hippocampal storage and/or retrieval of information (Gemmell et al. 2012; Maillet and Rajah 2011; Squire et al. 2004; Ta et al. 2012; Tubridy et al. 2011). The fact that performance as shown in Figure 10 was enhanced with respect the trial parameters of the task, i.e. 1) number of distracter images ($F(2,1682) = 7.78$, $p<0.001$) and 2) temporal delay between information exposure and retrieval ($F(2,1682) = 9.50$, $p<0.001$), supports the likelihood of enhancement of a process that facilitates information retrieval irrespective of the item specificity. Activation or Improvement of such a hippocampal process would provide recovery under conditions in which information encoding and retrieval was impaired, and as such serve as an effective prosthesis to restore degraded memory capacity in humans, as shown previously in rodents with pharmacologically induced hippocampal malfunction (Berger et al 2011). The presence of similar Strong codes (Figure 8) and their effectiveness when administered as MIMO derived electrical stimulation patterns under a wide range of memory conditions in all 4 NHPs (Figures 9&10), supports the development of the model as a generalized memory prosthesis. Since MIMO stimulation enhanced information encoding elevated performance relative to non-stimulation trials, the latter were therefore by comparison more difficult (Rolls et al. 2005). As such this application of the MIMO model clearly qualifies as a prosthetic type influence since performance, deterred by factors that directly affected retention, was improved by strong code MIMO stimulation in the same way in which it would operate if normal memory was impaired (Berger et al. 2011; Hampson et al. 2012c)

DISCUSSION

Retention of Task Specific Information Dependent on Hippocampal Encoding

For a number of years it has been established that the hippocampus is the primary memory structure in the mammalian brain (Cahusac et al. 1989; Malkova and Mishkin 2003; McEchron and Disterhoft 1999; Rolls et al. 2005). The basis for this principal evolves from both clinical and experimental evidence demonstrating the necessity of normal hippocampal function to provide memory capacity sufficient for daily existence in a complex society (Gold and Shadlen 2007; Pastalkova et al. 2008; Smith and Mizumori 2006; Squire et al. 2004). However two important features demonstrated in this study and recent prior studies from this program have not been previously described in primate hippocampus. The first new insight demonstrated here is the fact that information is encoded during the Sample phase trial-specifically in the primate hippocampus in a manner consistent with subsequent operation of the same neurons during the recall of that information in the Match phase of the same trial (Figures 2–4). Since the same CA1 and CA3 neurons are involved in both phases

of the memory process it is critical to understand how information is encoded by the multi-neuron system such that it can be extracted at a later time for decisions (Hampson et al 2012b). An important outcome in these investigations was that information encoding in the Sample phase determined the degree of success with respect to information retrieval and execution of the task in the subsequent Match phase. Hippocampal cells encoded specific details of information in the Sample phase for as long as 40 sec prior to utilization (Figures 2–4) and facilitated recall impaired with respect to as many as 6 other 'distracter' images (always leaving at least one position blank) during target selection (Figure 8). Therefore the manner in which information was encoded, as reflected by the MIMO derived strong code firing patterns, is a functionally specific feature of hippocampal circuitry that, 1) determines the degree to which other features in the Sample phase that are irrelevant to successful selection in the Match phase are excluded (Figure 5B) and 2) provides the resistance to decay of the relevant Sample encoded information over the subsequent intervening, random duration, delay period (Figure 5A).

Successful Performance Related to Hippocampal Encoding of Task Relevant Information

It is clear therefore that CA1 and CA3 firing in the Sample phase was the primary controlling factor in task performance, hence detection of that pattern of SR firing associated with successful trials provided a means of predicting and facilitating memory encoding during the task. The MIMO model accomplished this by detecting and classifying inter-related CA3-CA1 firing patterns as strong codes for supporting successful performance on the same trial as shown in Figure 8. The direct relationship between these MIMO extracted codes and task performance is exhibited in another conclusive manner by the relative interactive nature of strong codes for different types of trials as shown in Supplement Figure A (NHP1) in which 'weak codes' patterns on incorrect Object trials resembled 'strong code' patterns on successful Spatial trials. Therefore in addition to the difficulty incorporated by increased number of images and longer delays, retention was also required for the type of trial (Object or Spatial) designated by the trial start (TS) signal in the Sample phase of the task (Figures 1–2), and this also appeared to be incorporated in MIMO-derived CA3-CA1 Sample encoding patterns. The fact that animals had to deal with a large number of different types of trials randomly presented within the same session supports the possibility that extracted weak code patterns that caused errors were the result of miss-encoding with another strong code pattern for either a) a different type of trial or b) miss-anticipated parameters and is a logical interpretation of how overall task performance was controlled by the interaction of trial-specific MIMO-extracted patterns.

MIMO Model Induced Enhancement of Memory Encoding Under Difficult Circumstances

What is presented here is the first application of the MIMO model to primate hippocampus which is an extension of the application of the same model as a prosthesis to other primate brain areas, previously shown to be critical in controlling decision making in the Match phase in this same DMS task (Hampson et al. 2012a; Hampson et al. 2012b). However a previous successful application of a MIMO model prostheses to disrupted hippocampal neural processing in rodents (Berger et al., 2011, Hampson et al., 2012a) was the basis for employing this approach as a hippocampal neuroprosthesis for NHPs (Berger et al. 2011; Hampson et al. 2012a; Hampson et al. 2012c; Hampson et al. 2012d). In contrast to the application of MIMO model stimulation to the rodent hippocampus (Berger et al. 2011; Hampson et al. 2012a), the extent and range of effectiveness in improving cognitive performance in this NHP memory task was much greater (Figures 9&10). However, what is of major importance in regard to this demonstration of neuroprosthetic capability is the fact that, as in the rodent model (Berger et al 2011), effective CA1 stimulation parameters had to mimic those derived by the MIMO model which represented CA3-CA1 firing sampled during strong encoding of trial-specific sample information. This was confirmed by

stimulating the same CA1 location with different (i.e. scrambled strong code coefficients) patterns of pulses at the same intensities (Figure 10) which did not facilitate performance. Therefore, the Strong code patterns extracted by the MIMO model were not only effective because they mimicked firing on successful trials, they also were capable of increasing performance above control levels due to delivery on trials in which ineffective (weak) encoding (errors) occurred (Figures 9&10). Hence, these results demonstrate the potential for MIMO stimulation delivered in strong code patterns to primate hippocampus, to not only facilitate but also recover memory in subjects, including humans, impaired by pathological events such as brain damage, or even brain aging where memory disruption is more or less permanent (Carmichael et al. 2012; Gemmell et al. 2012; Maillet et al. 2011; Riddle et al. 2007; Ta et al. 2012).

Conclusions

These unique results are the first to show that interactions between CA3 and CA1 hippocampal neurons in primate brain that encode information relevant to successful performance of a memory-dependent decision making task (Deadwyler et al. 2007; Porrino et al. 2005) are capable of being extracted and re-introduced via application of a MIMO model neuroprosthesis (Berger et al. 2011; Hampson et al. 2012a) as demonstrated here. The neural basis for effective performance in this task likely relates to significantly increased synaptic transmission from CA3-CA1 in hippocampus (Song et al. 2007; Song et al. 2009) to encode proper information during the Sample phase (Figures 8&9). Therefore interposing a MIMO model to control this type of processing provides a means of reducing random fluctuations in performance under normal conditions (Figures 5&8) and/or to recover performance when retention is reduced or impaired (Figures 9&10). In addition to providing potential insight into other types of cognitive impairments involving decision making and executive function in human brain as a result of disease or injuries (Gold et al. 2007; Graybiel 2008; Wang et al. 2011), these results provide confirmation that a MIMO-based functional device, integrated physiologically with hippocampal operation will improve and even recover lost memory capacity in humans affected with similar disorders.

Supplementary Material

Refer to Web version on PubMed Central for supplementary material.

Acknowledgments

We thank Joshua Long, Joseph Noto, Brian Parish, and Christina Dyson for their dedication and technical expertise in conducting this project. This work was supported by National Institutes of Health Grants DA06634, DA023573, DA026487 (to S.A.D.) and by Defense Advanced Research Projects Agency (DARPA) contracts N66001-09-C-2080 (to S.A.D.) and N66001-09-C-2081 (to T.W.B.). This work was also supported in part by grants NSF EEC-0310723 (to T.W.B.), and NIH/NIBIB grant No. P41-EB001978 to the Biomedical Simulations Resource at USC (V.Z.M. and T.W.B.).

References

Berger TW, Hampson RE, Song D, Goonawardena A, Marmarelis VZ, Deadwyler SA. A cortical neural prosthesis for restoring and enhancing memory. Journal of Neural Engineering. 2011; 8:046017. [PubMed: 21677369]

Berger TW, Song D, Chan RH, Marmarelis VZ, LaCoss J, Wills J, Hampson RE, Deadwyler SA, Granacki JJ. A hippocampal cognitive prosthesis: multi-input, multi-output nonlinear modeling and VLSI implementation. IEEE Trans Neural Syst Rehabil Eng. 2012; 20:198–211. [PubMed: 22438335]

Cahusac PM, Miyashita Y, Rolls ET. Responses of hippocampal formation neurons in the monkey related to delayed spatial response and object-place memory tasks. Behav Brain Res. 1989; 33:229–240. [PubMed: 2757782]

Carmichael O, Xie J, Fletcher E, Singh B, DeCarli C. Localized hippocampus measures are associated with Alzheimer pathology and cognition independent of total hippocampal volume. Neurobiol Aging. 2012; 33:1124–1141. [PubMed: 22169204]

Deadwyler SA, Porrino L, Siegel JM, Hampson RE. Systemic and nasal delivery of orexin-A (Hypocretin-1) reduces the effects of sleep deprivation on cognitive performance in nonhuman primates. J Neurosci. 2007; 27:14239–14247. [PubMed: 18160631]

Deguchi Y, Donato F, Galimberti I, Cabuy E, Caroni P. Temporally matched subpopulations of selectively interconnected principal neurons in the hippocampus. Nat Neurosci. 2011; 14:495–504. [PubMed: 21358645]

Downes JJ, Mayes AR, MacDonald C, Hunkin NM. Temporal order memory in patients with Korsakoff's syndrome and medial temporal amnesia. Neuropsychologia. 2002; 40:853–861. [PubMed: 11900736]

Eichenbaum H, Fortin N. Episodic Memory and the Hippocampus: It's About Time. Current Directions in Psychological Science. 2003; 12:53–57.

Gemmell E, Bosomworth H, Allan L, Hall R, Khundakar A, Oakley AE, Deramecourt V, Polvikoski TM, O'Brien JT, Kalaria RN. Hippocampal neuronal atrophy and cognitive function in delayed poststroke and aging-related dementias. Stroke. 2012; 43:808–814. [PubMed: 22207507]

Gold JI, Shadlen MN. The neural basis of decision making. Annu Rev Neurosci. 2007; 30:535–574. [PubMed: 17600525]

Graybiel AM. Habits, rituals, and the evaluative brain. Annu Rev Neurosci. 2008; 31:359–387. [PubMed: 18558860]

Hampson RE, Espana RA, Rogers GA, Porrino LJ, Deadwyler SA. Mechanisms underlying cognitive enhancement and reversal of cognitive deficits in nonhuman primates by the ampakine CX717. Psychopharmacology (Berl). 2009; 202:355–369. [PubMed: 18985324]

Hampson RE, Gerhardt GA, Marmarelis VZ, Song D, Opris I, Santos L, Berger TW, Deadwyler SA. Facilitation and restoration of cognitive function in primate prefrontal cortex by a neuroprosthesis that utilizes minicolumn-specific neural firing. J Neural Eng. 2012a; 9:056012. [PubMed: 22976769]

Hampson RE, Opris I, Deadwyler SA. Neural correlates of fast pupil dilation in nonhuman primates: relation to behavioral performance and cognitive workload. Behavioral Brain Research. 2010; 212:1–11.

Hampson RE, Opris I, Song D, Gerhardt GA, Shin D, Marmarelis VZ, Berger TW, Deadwyler SA. Neural representation of cognitive processing in the prefrontal cortex of nonhuman primates. Conf Proc IEEE Eng Med Biol Soc. 2012b

Hampson RE, Pons TP, Stanford TR, Deadwyler SA. Categorization in the monkey hippocampus: A possible mechanism for encoding information into memory. Proc Natl Acad Sci USA. 2004; 101:3184–3189. [PubMed: 14978264]

Hampson RE, Porrino LJ, Opris I, Stanford T, Deadwyler SA. Effects of cocaine rewards on neural representations of cognitive demand in nonhuman primates. Psychopharmacology (Berl). 2011; 213:105–118. [PubMed: 20865250]

Hampson RE, Song D, Chan RH, Sweatt AJ, Riley MR, Gerhardt GA, Shin DC, Marmarelis VZ, Berger TW, Deadwyler SA. A nonlinear model for hippocampal cognitive prosthesis: memory facilitation by hippocampal ensemble stimulation. IEEE Trans Neural Syst Rehabil Eng. 2012c; 20:184–197. [PubMed: 22438334]

Hampson RE, Song D, Chan RH, Sweatt AJ, Riley MR, Goonawardena AV, Marmarelis VZ, Gerhardt GA, Berger TW, Deadwyler SA. Closing the loop for memory prosthesis: detecting the role of hippocampal neural ensembles using nonlinear models. IEEE Trans Neural Syst Rehabil Eng. 2012d; 20:510–525. [PubMed: 22498704]

Jenkins LJ, Ranganath C. Prefrontal and medial temporal lobe activity at encoding predicts temporal context memory. J Neurosci. 2010; 30:15558–15565. [PubMed: 21084610]

Klausberger T, Somogyi P. Neuronal diversity and temporal dynamics: the unity of hippocampal circuit operations. Science. 2008; 321:53–57. [PubMed: 18599766]

Maillet D, Rajah MN. Age-related changes in the three-way correlation between anterior hippocampus volume, whole-brain patterns of encoding activity and subsequent context retrieval. Brain Research. 2011; 1420:68–79. [PubMed: 21945346]

Malkova L, Mishkin M. One-trial memory for object-place associations after separate lesions of hippocampus and posterior parahippocampal region in the monkey. J Neurosci. 2003; 23:1956–1965. [PubMed: 12629201]

Manns JR, Howard MW, Eichenbaum H. Gradual changes in hippocampal activity support remembering the order of events. Neuron. 2007; 56:530–540. [PubMed: 17988635]

Marmarelis, VZ. Nonlinear Dynamic Modeling of Physiological Systems. Hoboken, NJ: Wiley-IEEE Press; 2004.

Marmarelis VZ, Berger TW. General methodology for nonlinear modeling of neural systems with Poisson point-process inputs. Math Biosci. 2005; 196:1–13. [PubMed: 15963534]

Marmarelis VZ, Shin DC, Hampson RE, Deadwyler SA, Song D, Berger TW. Design of optimal stimulation patterns for neuronal ensembles based on volterra-type hierarchical modeling. J Neural Eng. 2012; 9:066003. [PubMed: 23075519]

Marmarelis VZ, Shin DC, Song D, Hampson RE, Deadwyler SA, Berger TW. Nonlinear modeling of dynamic interactions within neuronal ensembles using Principal Dynamic Modes. J Comput Neurosci. 2013; 34:73–87. [PubMed: 23011343]

McEchron MD, Disterhoft JF. Hippocampal encoding of non-spatial trace conditioning. Hippocampus. 1999; 9:385–396. [PubMed: 10495020]

Moscovitch M, Nadel L, Winocur G, Gilboa A, Rosenbaum RS. The cognitive neuroscience of remote episodic, semantic and spatial memory. Current Opinion in Neurobiology. 2006; 16:179–190. [PubMed: 16564688]

Naya Y, Suzuki WA. Integrating what and when across the primate medial temporal lobe. Science. 2011; 333:773–776. [PubMed: 21817056]

Opris I, Fuqua JL, Huettl PF, Gerhardt GA, Berger TW, Hampson RE, Deadwyler SA. Closing the loop in primate prefrontal cortex: inter-laminar processing. Front Neural Circuits. 2012a; 6:88. [PubMed: 23189041]

Opris I, Hampson RE, Deadwyler SA. The encoding of cocaine vs. natural rewards in the striatum of nonhuman primates: Categories with different activations. Neuroscience. 2009; 163:195–204.

Opris I, Hampson RE, Gerhardt GA, Berger TW, Deadwyler SA. Columnar processing in primate prefrontal cortex: Evidence for executive control microcircuits. J Cogn Neurosci. 2012b; 24:2334–2347. [PubMed: 23016850]

Opris I, Hampson RE, Stanford TR, Gerhardt GA, Deadwyler SA. Neural activity in frontal cortical cell layers: evidence for columnar sensorimotor processing. J Cogn Neurosci. 2011; 23:1507–1521. [PubMed: 20695762]

Pastalkova E, Itskov V, Amarasingham A, Buzsaki G. Internally generated cell assembly sequences in the rat hippocampus. Science. 2008; 321:1322–1327. [PubMed: 18772431]

Porrino LJ, Daunais JB, Rogers GA, Hampson RE, Deadwyler SA. Facilitation of task performance and removal of the effects of sleep deprivation by an ampakine (CX717) in nonhuman primates. PLoS Biol. 2005; 3:e299. [PubMed: 16104830]

Riddle, DR.; Lichtenwalner, RJ. Neurogenesis in the Adult and Aging Brain. In: Riddle, DR., editor. Brain Aging: Models, Methods, and Mechanisms (Frontiers in Neuroscience). Boca Raton (FL): CRC Press; 2007.

Rolls ET, Xiang J, Franco L. Object, space, and object-space representations in the primate hippocampus. J Neurophysiol. 2005; 94:833–844. [PubMed: 15788523]

Smith DM, Mizumori SJ. Learning-related development of context-specific neuronal responses to places and events: the hippocampal role in context processing. J Neurosci. 2006; 26:3154–3163. [PubMed: 16554466]

Song D, Chan RH, Marmarelis VZ, Hampson RE, Deadwyler SA, Berger TW. Nonlinear dynamic modeling of spike train transformations for hippocampal-cortical prostheses. IEEE Trans Biomed Eng. 2007; 54:1053–1066. [PubMed: 17554824]

Song D, Chan RH, Marmarelis VZ, Hampson RE, Deadwyler SA, Berger TW. Nonlinear modeling of neural population dynamics for hippocampal prostheses. Neural Netw. 2009; 22:1340–1351. [PubMed: 19501484]

Squire, LR.; Clark, RE.; Bailey, PJ. Medial temporal lobe function and memory. In: Gazzaniga, M., editor. The Cognitive Neuroscience III. Cambridge, MA: MIT Press; 2004. p. 691-708.

Ta AT, Huang SE, Chiu MJ, Hua MS, Tseng WY, Chen SH, Qiu A. Age-related vulnerabilities along the hippocampal longitudinal axis. Hum Brain Mapp. 2012; 33:2415–2427. [PubMed: 21898676]

Tubridy S, Davachi L. Medial temporal lobe contributions to episodic sequence encoding. Cereb Cortex. 2011; 21:272–280. [PubMed: 20494967]

Tulving E. Episodic memory: from mind to brain. Annu Rev Psychol. 2002; 53:1–25. [PubMed: 11752477]

Wang M, Gamo NJ, Yang Y, Jin LE, Wang XJ, Laubach M, Mazer JA, Lee D, Arnsten AF. Neuronal basis of age-related working memory decline. Nature. 2011; 476:210–213. [PubMed: 21796118]

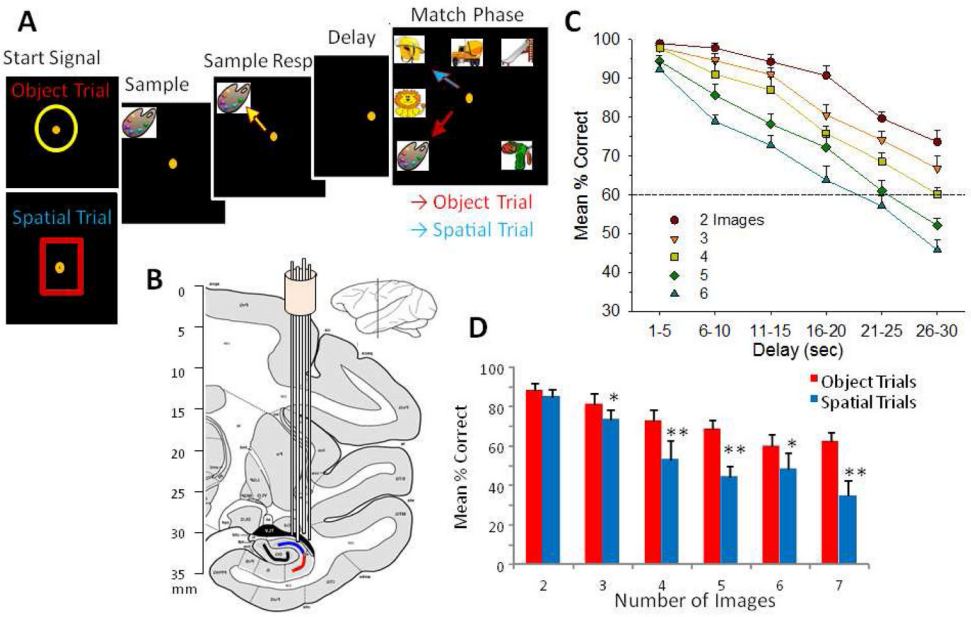

Figure 1.

Illustration of Delayed Match to Sample (DMS) Behavioral Task and Localization of Hippocampal Recording Electrodes. **A.** Behavioral paradigm showing sequence of events in the DMS task presented on screen with correct cursor movement (orange dot) indicated for each phase of the task commencing with: 1) 'Start Signal' presentation consisted of either yellow circle (upper) or red square (lower) signaling Object or Spatial trial, respectively. Placement of the cursor into the Start Signal initiated the trial commencing with: 2) Presentation of the 'Sample clipart Image' in one of 8 different locations on the screen. 3) Sample Response consisted of movement of the cursor onto the Sample image. 4) Variable 'Delay' period of 1–40 sec followed the Sample Response, during which the screen was blank. 5) Match Phase followed Delay timeout, in which the "Match clipart image" (same as the Sample image) was presented randomly in one of eight locations on the screen accompanied by 1–6 other distracter (Non-Match) images in other locations on the same screen. Cursor movements onto trial-appropriate response targets in the Match phase, either a) the same Sample image (Object trial, red arrow) or b) the same location on the screen where the Sample Response was made irrespective of image identity (Spatial trial, blue arrow), were rewarded by delivery of a squirt of juice reward. Placement of the cursor onto a Non-match (distracter) image (Object trial) or onto a different screen location from the Sample Response (Spatial trial) caused the screen to go blank without reward delivery. Intertrial interval (ITI): 10.0s. **B.** Diagram of NHP brain in cross section showing hippocampal tetrode tracks through temporal lobe and placement in the CA3 and CA1 cell layers. **C.** Overall performance averages showing interaction of interposed delays on task performance as a function of number of distracter images on Object trials. Dotted line at 60% is a marker below which performance is near chance levels. **D.** Differential mean % correct performance on Object and Spatial trials (blue and red arrows in "A") as a function of the number of (distracter) images presented in the Match phase of the task.

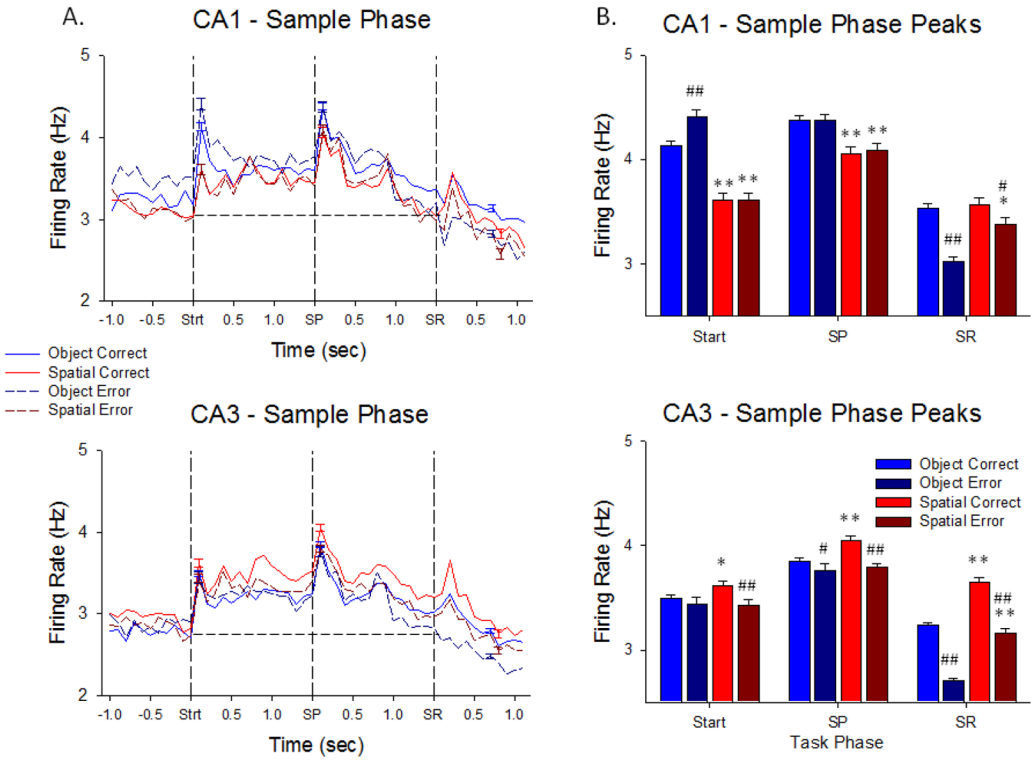

Figure 2.

Hippocampal neuron firing in the Sample Phase of the DMS task. **A.** Upper (CA1 cells, n= 431) and lower (CA3 cells, n= 801) plots show trial-based histograms (TBHs) of average firing of all cells in those cell layers, across all NHPs (n=4). Each trace indicates one of the 4 conditions listed on the left for comparison of Object vs. Spatial and Correct vs. Error trials. The three events within the Sample phase are listed on the x-axis and shown as vertical dotted lines of each TBH as: Strt = Start Signal; SP = Sample Image Presentation; SR = Sample Response. Horizontal dotted lines provide a basis for comparing mean firing levels prior to onset of the Sample Phase, in terms of each of the three mean peaks as significantly increased over baseline by standard scores ($Z>3.09$, $p<0.001$, see Methods). Trials were sorted by Object/Spatial/Correct/Error trials, with mean percent correct performance calculated per session, and averaged across animals (n=4) and sessions (n>5 per animal). **B.** Plots of mean peak responses to the same 3 Sample phase events across the same 4 trial conditions shown in A for CA1 (upper) and CA3 (lower) neurons summed over all 4 animals to indicate relations of overall firing tendencies and differential encoding under different task conditions including correct and error trials. *$*p<0.01$, **$*p<0.001$ Object vs. Spatial trial peaks, $^{\#}p<0.01$, $^{\#\#}p<0.001$ Correct vs. Error trial peaks.*

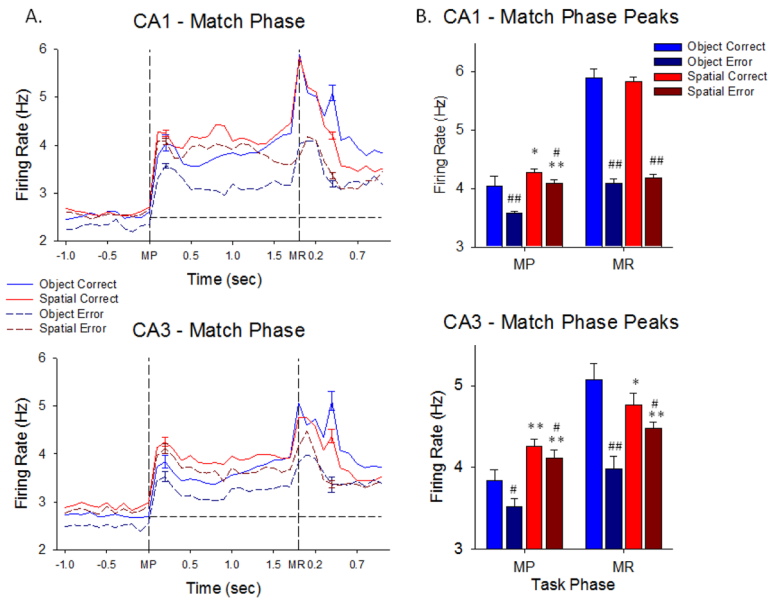

Figure 3.

Hippocampal neuron firing in the Match Phase of the DMS task. **A.** TBH plots as in Figure 2A show trial-based histograms of average firing of CA1 and CA3 neurons during the Match phase of the DMS task. The two task events indicated by the vertical dotted lines were 1) Match screen presentation (MP) occurring at the end of the prior variable delay period, and then 2) the subsequent Match phase response (MR) for correct vs. incorrect selection of the Sample feature executed in the presence of other 1–6 other images. Each peak was significantly increased over baseline by standard scores ($Z>3.09$, $p<0.001$, see Methods). The peaks with error bars after the MR occurred on correct trials when the juice reward valve sounded. Plots reflect sustained elevated mean firing rates throughout the entire Match Phase for both CA1 and CA3 hippocampal cells in each of the 4 indicated conditions with respect to screen presentation of images and performance of that type of trial. **B.** Average peak firing rates of CA1 and CA3 hippocampal cells in the Match phase shown for each of the events (MP, MR) in each trial type (Object and Spatial) sorted with respect to performance (correct and error) on the same trials. *$*p<0.01$, **$*p<0.001$ Object vs. Spatial trial peaks, $^{\#}p<0.01$, $^{\#\#}p<0.001$ Correct vs. Error trial peaks.*

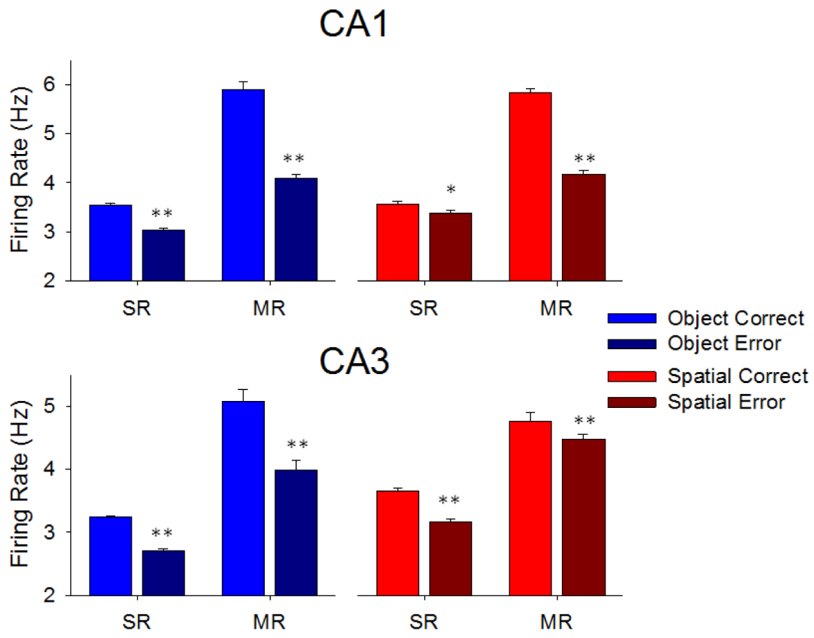

Figure 4.

Overall average firing of hippocampal CA1 (upper) and CA3 (lower) neurons during Sample and Match Responses reflect correct and error performance outcome on different types of DMS trials. Mean firing rates during Sample (SR) and Match (MR) Reponses were computed on correct and error trials summed over all NHPs for Object (N=4) and Spatial (N=3) trials. Mean firing rates during the MR were consistently higher than SR for both trial types but significantly higher for both SR and MR on correct vs. error trials under all conditions. **p<0.01, **p<0.001 Correct vs. Error trial peaks.*

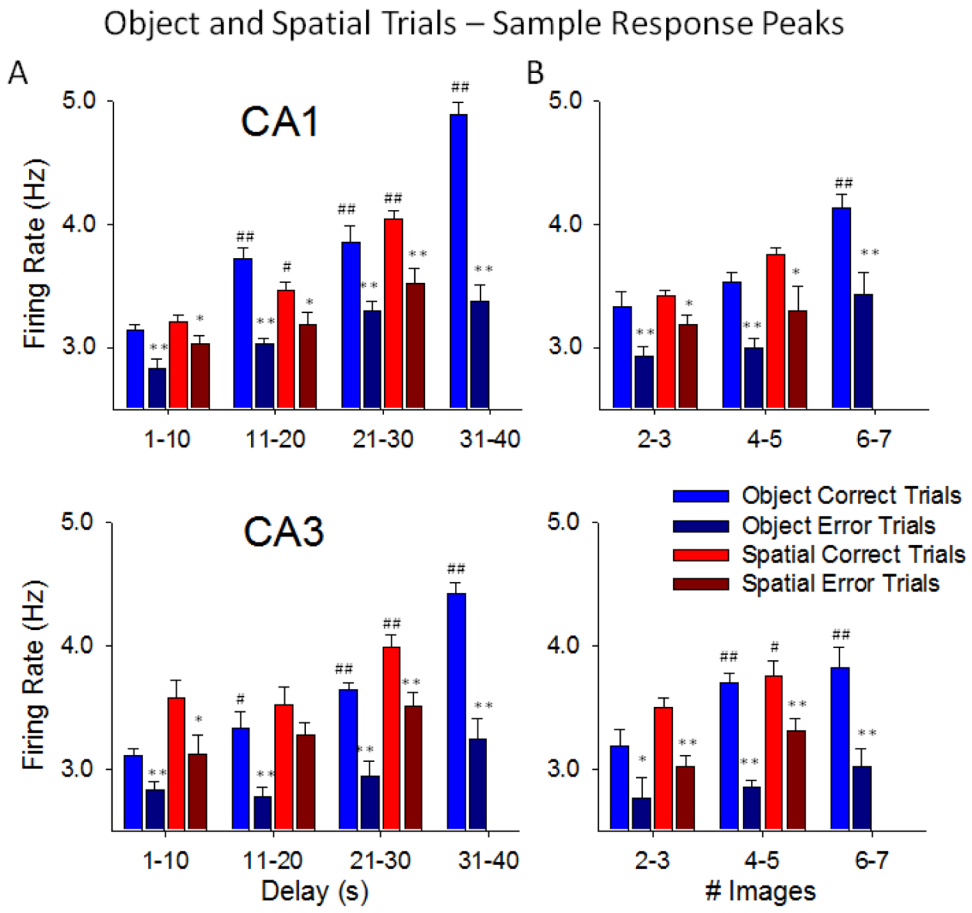

Figure 5.

Trial specific consequences of Sample Response (SR) encoding by hippocampal neurons over all trial parameters. **A.** Average peak firing of CA1 (upper) and CA3 (lower) neurons during the SR on Object and Spatial trials with respect to the subsequent trial delay and performance outcome on the same trial. Each plot shows the differential relationship of SR mean firing rate to trial outcome (correct vs. error) sorted by the duration of the delay interval (1–40s) on the same trial. Trials were sorted by delays grouped in 10 s intervals; mean percent correct performance per session was then averaged across animals (n=4) and sessions (n>5 per animal). **p<0.01, **p<0.001 vs. Correct trial peaks, #p<0.01, ##p<0.001 vs. 1–10 s Delays.* **B.** Average peak neuron firing during the SR as in **A** plotted as a function of number of Match Phase images and performance outcome. Differential relationship of SR encoding to trial outcome (correct vs. error) sorted by the subsequent number of images (2–7) presented in the subsequent Match phase on the same trial. Trials were grouped and plotted in progressive 2 image intervals; mean percent correct performance was then averaged across animals (n=4) and sessions (n>5 per animal). **p<0.01, **p<0.001 vs. Correct trial peaks, #p<0.01, ##p<0.001 vs. 2–3 Images.* Spatial trials are not shown for delays of 31–40s and 6–7 distracter images because none of the NHPs were capable of performing trials with these parameters efficiently under this contingency.

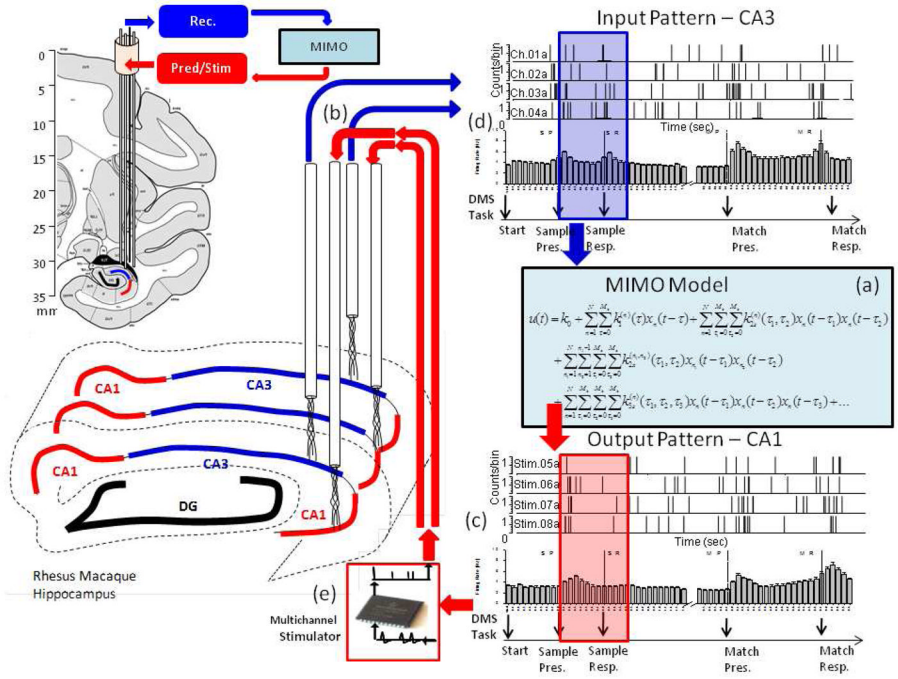

Figure 6.

Integration of Multi-input, multi-output (MIMO) nonlinear model (a) to calculate SR encoding via spatiotemporal firing relations between hippocampal CA3 and CA1 recordings (b), to predict CA1 firing (c) from CA3 recordings (d), and generate patterned stimulation (e) for feedback to Layer CA1. The anatomical diagrams at the left show placement of CA3 and CA1 multi-cell recording tetrodes into the associated transverse fields along the longitudinal axis of hippocampus. The recordings on correct DMS trials from these spatially distinct and layer specific tetrodes were fed into the MIMO model with CA3 as the input (blue arrow) and CA1 as the output pattern (red arrow). The MIMO model predicted correct CA1 output (i.e. “Strong Codes”) from CA3 input computed over the Sample Phase (shaded rectangles) based on fine temporal relationships between spike trains recorded on correct trials at different spatial locations within hippocampus. On stimulation trials, trains of electrical pulses mimicking the predicted Strong Code output spike trains were delivered to the same CA1 hippocampal electrode locations the patterns were recorded from. MIMO model controlled stimulation patterns applied to the respective CA1 recording locations consisted of multi-channel biphasic pulses of 10–50 μA, 1.0 ms duration with a minimum 50 ms between stimulation pulses, with no more than 20 stimulation pulses per second per channel.

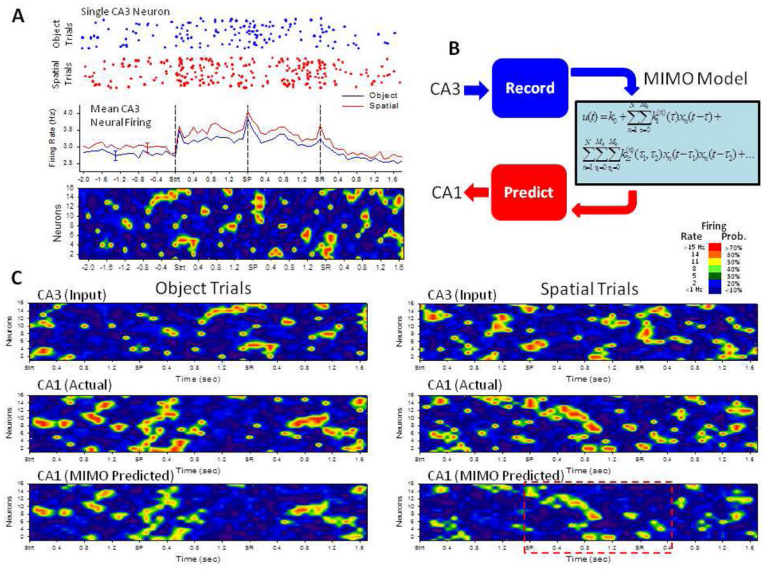

Figure 7.

Operation of MIMO model as an input-output function of CA3 and CA1 firing. **A.** Rastergram at top illustrates firing of a single CA3 neuron on successive Object (blue) and Spatial (red) trials. Each dot indicates single action potential firing or "spike"; each row indicates firing on a single trial synchronized to the same temporal axis as TBHs below. The Heat map display underneath depicts mean firing rate averaged across trials in a single session for 16 CA3 neurons plotted on the same time scale as the TBHs from Fig. 2A, in relation to the same Sample phase events (Strt., SP, SR). The Heat-map color codes spike train firing rate in 100 ms bins ranging from <1 Hz (dark blue) to >15 Hz (red). **B.** Diagram shows that MIMO model predicts CA1 spike train output as a nonlinear function of CA3 spike train input as described in text. **C.** Heat-map Illustration of directly recorded CA3 and directly recorded ("Actual") CA1 spike trains shown in comparison to MIMO-predicted CA1 spike trains over the same temporal sequences for both Object and Spatial trials. Heat-maps depict spike trains from a single trial of the same type to demonstrate fidelity of the MIMO predicted CA1 outputs (scaled as probability of firing, see scale inset) compared to actual CA1 firing. The dashed red rectangle in the lower right Heat-map indicates the trial period (SP to SR) corresponding to the Sample codes presented in Figure 8.

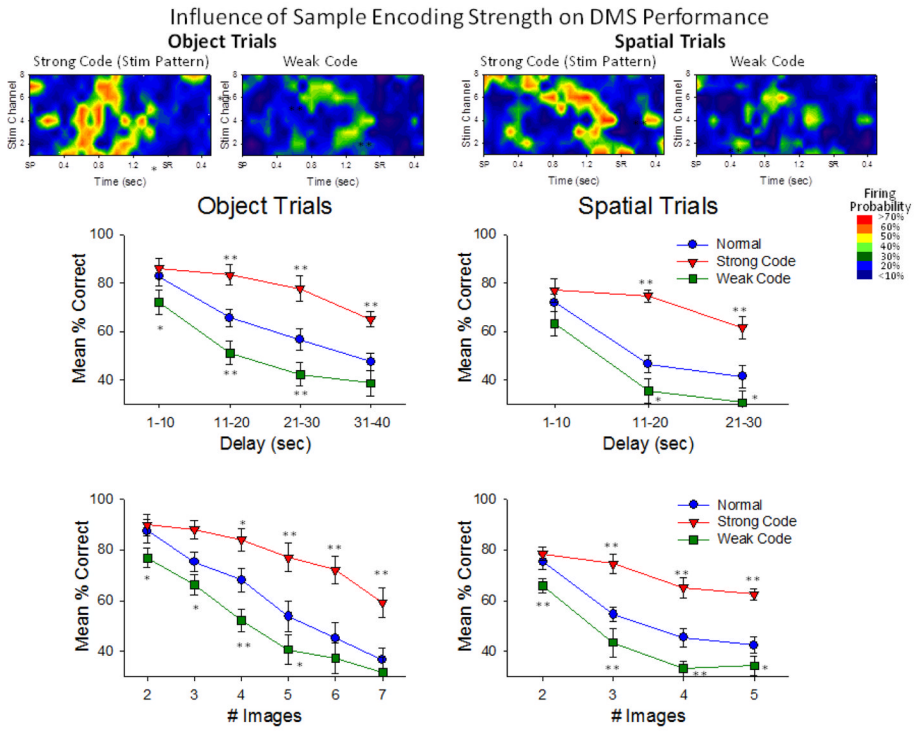

Figure 8.

Influence of MIMO-predicted Sample encoding strength on DMS performance. The upper Heat-map rasters show the CA1 firing patterns (see Fig. 7, dashed red rectangle) extracted by the MIMO model on correct (Strong code) and incorrect (Weak code) trials for both Object and Spatial trials. Strong codes were obtained from averaging of MIMO-derived CA1 spike trains on correctly-performed trials of high difficulty (21–30s delays, 6–7 Match phase images), while Weak codes were obtained from averaging MIMO-derived CA1 spike trains on incorrectly-performed less difficult trials (1–10 delays, 2–3 Match phase images). Heat-map colors encode mean firing probability from MIMO model rate: <10% (blue) to >70% (red) as shown in inset. Plots below the Heat-maps are graphs that show mean % correct behavioral performance on Object and Spatial trials. Normal: performance not sorted according to strength of Sample encoding on the trial (non-defined encoding). Strong Code: MIMO-derived SR firing constituted Strong codes on each trial. Weak Code: MIMO-derived SR firing constituted Weak Codes on each trial. Performance under these three conditions was sorted as a function of the length of the delay (upper), or number of images in the Match phase of the task (lower). **p<0.01, **p<0.001 vs. Normal.*

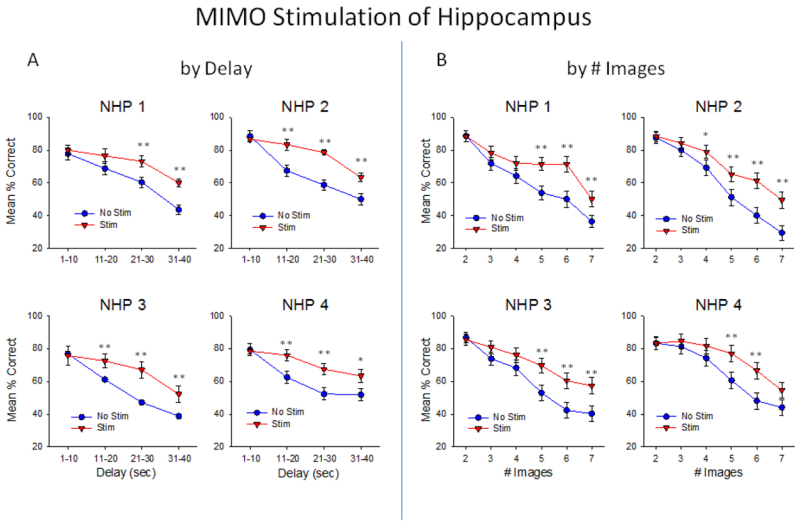

Figure 9.

Facilitation of DMS performance by MIMO strong code CA1 hippocampal stimulation. Each graph shows the difference in performance on stimulated vs. nonstimulated trials as a function of duration of the intervening delay (**A**) and #images (**B**) for each individual NHP subject in which Strong code stimulus patterns to CA1 areas were delivered randomly in the Sample phase with respect to trial types during the same sessions. Stimulation was delivered on 30–50% of trials, resulting in 40–50 stim trials per session, and 80–100 non-stimulated trials in the same sessions (3–4 sessions per NHP subject). **p<0.01, **p<0.001 Stim vs. No Stim*.

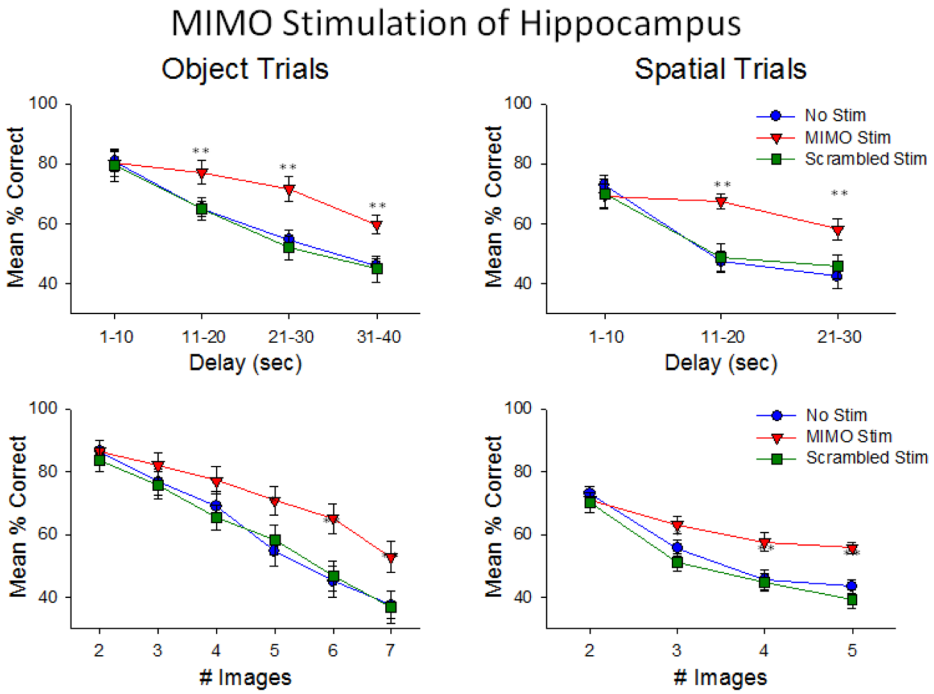

Figure 10.

Effects of Specificity of MIMO-derived stimulation as a function of type of DMS trial. Performance levels averaged over all animals are shown for both Object (left) and Spatial (right) trials with respect to intervening delay (upper) and #images (lower). Performance facilitation on MIMO Scrambled Stim trials was not above that on No Stim trials. On Scrambled Stim trials patterns in which MIMO coefficients were randomized with respect to neuron and time had little or no effect and did not disrupt normal performance. Since only MIMO Strong code patterns were used to generate the Scrambled Stim patterns, they were not functionally equivalent to the weak code patterns shown in Figure 8. *$p<0.01$, **$p<0.001$ Stim vs. No Stim.*